EFFECTS OF CHLORIDE ON COPPER CORROSION

Prepared for

U.S. Nuclear Regulatory Commission
Contract NRC–HQ–12–C–02–0089

Prepared by

Xihua He[1]
Tae Ahn[2]

[1]Center for Nuclear Waste Regulatory Analyses
San Antonio, Texas

[2]U.S. Nuclear Regulatory Commission
Washington, DC

July 2018

ABSTRACT

Copper (Cu) is one of the candidate waste container materials for high-level radioactive waste geologic disposal systems located in the saturated zone, because of its thermodynamic stability in anoxic water. However, species in the groundwater could change its stability and electrochemical properties, especially corrosion resistance. This study investigated the role of chloride (Cl^-) in Cu corrosion in solutions containing sulfate (SO_4^{2-}) and Cl^- with residual O_2 concentration of about 0.1–0.2 ppb at 50 °C [122 °F]. SO_4^{2-} concentration was kept constant at 2×10^3 ppm, while Cl^- concentration was varied from 0 to 1×10^3, 1×10^4, and 1×10^5 ppm. Electrochemical methods, including corrosion potential (E_{corr}) monitoring, potentiodynamic polarization, and electrochemical impedance spectroscopy (EIS), were used to study the electrochemical properties of Cu affecting corrosion resistance.

All the results obtained from different methods consistently demonstrate that Cl^- and temperature play significant roles in enhancing corrosion of copper when the O_2 concentration is extremely low. E_{corr} decreased with increasing Cl^- concentration and was lower at 50 °C [122 °F] than at 20 °C [68 °F]. During both forward and reverse potentiodynamic polarization scans, E_{corr} consistently decreased and the current density increased with increasing Cl^- concentration. Tafel slopes from the forward scan regions decreased and the exchange current density increased with increasing Cl^- concentration. The EIS data differed in solutions with different Cl^- concentration levels and they became more complex at elevated temperature. A layered film structure was inferred from the EIS data. Polarization resistance derived by fitting to the EIS data was the lowest at the highest Cl^- concentration, which is consistent with increasing corrosion rates with increasing Cl^- concentration. Uncertainty remains with regard to the composition and structure of the films formed from the corrosion process, the cathodic reactions that support the corrosion process, and their implications for long-term performance under repository conditions. Further work is needed to evaluate (i) the corrosion products using more sensitive analytical methods and (ii) the cathodic reactions that support the corrosion process in deep geologic repository environments.

CONTENTS

FIGURES

FIGURES (Continued)

TABLES

ACKNOWLEDGMENTS

This report was prepared to document work performed by the Center for Nuclear Waste Regulatory Analyses (CNWRA®) for the U.S. Nuclear Regulatory Commission (NRC) under Contract No. NRC–HQ–12–C–02–0089. The activities reported here were performed on behalf of the NRC Office of Nuclear Material Safety and Safeguards, Division of Spent Fuel Management. The report is an independent product of CNWRA and does not necessarily reflect the views or regulatory position of NRC. The NRC staff views expressed herein are preliminary and do not constitute a final judgment or determination of the matters addressed or of the acceptability of any licensing action that may be under consideration at NRC.

The authors acknowledge the valuable contributions of the NRC Project Manager, J. Gwo, for guidance, feedback, and information provided over the duration of this project.

The authors thank B. Werling for support in achieving stable and inert atmosphere conditions in the glovebox, O. Pensado for technical review, and D. Pickett for programmatic review. The authors also thank A. Ramos for support in report preparation and editorial review.

QUALITY OF DATA, ANALYSES, AND CODE DEVELOPMENT

DATA: All CNWRA-generated original data contained in this report meet the quality assurance requirements described in the CNWRA Quality Assurance Manual. Sources for other data should be consulted for determining the level of quality for those data. Scientific Notebook 1312 (He, 2018) documents experimental conditions.

ANALYSES AND CODES: none

REFERENCES:

He. X. "Copper and Carbon Steel Experiments." Scientific Notebook 1312. San Antonio, Texas: Center for Nuclear Waste Regulatory Analyses. pp. 1–51. 2018.

1 INTRODUCTION

Many countries have been exploring the feasibility of high-level waste (HLW) disposal in deep geologic repositories, including Switzerland, Sweden, Finland, Japan, and Canada (King, 2013). Copper (Cu) is one of the candidate metallic materials for waste containment. After hundreds of years, the deep groundwater in these potential repositories may evolve from oxic to anoxic conditions, under which corrosion rates of Cu are expected to be low. However, species in the groundwater such as chloride (Cl^-) and sulfide (S^{2-}) could change Cu thermodynamic stability and electrochemical properties, especially corrosion resistance. Furthermore, elevated temperatures induced by HLW decay heat release could also affect these material properties. In Fiscal Year (FY) 2017, He and Ahn (2018) evaluated the effects of Cl^- on Cu corrosion over a concentration range from 0 to 10^5 ppm Cl^- at 20 °C [68 °F]. The study showed that a two orders of magnitude increase in Cl^- concentration led to a less than one order of magnitude increase in corrosion rate; all Cu corrosion rates were below 10 nm/yr [4×10^{-7} in/yr]. The work reported here, conducted in FY 2018, continued the evaluation of the effects of Cl^- on Cu corrosion, but at a higher temperature. Cu corrosion tests were conducted in solutions with O_2 concentrations of 0.1–0.2 ppb containing common species—such as sodium ion (Na^+), calcium ion (Ca^{2+}), Cl^-, and sulfate (SO_4^{2-})—found in most deep groundwater. The specific objective of this work was to evaluate the effects of Cl^- on Cu corrosion at 50 °C [122 °F] for comparison with the results at 20 °C [68 °F].

2 EXPERIMENTAL APPROACHES

The test matrix is shown in Table 1. Tests were conducted in 4 solutions at 50 °C [122 °F]. The SO_4^{2-} concentration was kept constant at 2×10^3 ppm by adding sodium sulfate (Na_2SO_4). The Cl^- concentration was varied from 0 to 1×10^3, 1×10^4, and 1×10^5 ppm by adding a constant amount of calcium chloride ($CaCl_2$) (except for the zero Cl^- solution), and a varying amount of sodium chloride (NaCl). All the tests were conducted in a Labconco® controlled atmosphere glovebox, which provided a leak tight and inert atmosphere. This same glovebox was used for the FY 2017 work reported in He and Ahn (2018). The measured O_2 level in the glovebox during the tests was 3–6 ppm. The O_2 scrubber that maintains the low O_2 level was refreshed once every month to ensure its optimum function. Based on a Henry's law constant of 1.3×10^{-3} mol/(L·atm) in fresh water at room temperature (Sander, 2015), the O_2 solution concentration was about 0.1–0.2 ppb. Because oxygen solubility is negatively correlated with temperature and the quantity of dissolved solids, oxygen solubility under the test conditions is expected to be even lower than 0.1–0.2 ppb.

The tests used oxygen-free high conductivity copper cylindrical electrodes, which were fabricated from the same batch of material used in all previous work (He et al., 2015; He and Ahn, 2017; He and Ahn, 2018). Except for the test in Solution 2, a second copper electrode was set in the solution for a partial duplicated test to check reproducibility. The corrosion potential (E_{corr}) was monitored and electrochemical impedance spectroscopy (EIS) data were collected after several days of E_{corr} monitoring. For the four tests shown in Table 1, the test duration ranged from 20 to 28 days. EIS measurements were performed using a Gamry potentiostat. All measurements were performed with the potential held at the value of E_{corr} using a perturbation voltage signal of 10 mV applied over the frequency range from 10^{-3} to 10^5 Hz. Ten data points per decade were recorded. At the end of the tests, a cyclic potentiodynamic

Table 1. Test matrix on evaluating effects of chloride on Cu corrosion						
Cell	**Solution #**	**Na_2SO_4 (mol/L)**	**$CaCl_2$ (mol/L)**	**NaCl (mol/L)**	**T, °C**	**Methods**
Glass cell set up in glovebox under inert atmosphere	1	0.02*	0	0	50†	Corrosion potential, electrochemical impedance spectroscopy, and potentiodynamic polarization
	2	0.02	0.01	0.008	50	
	3	0.02	0.01	0.26	50	
	4	0.02	0.01	2.8	50	

*This concentration makes 2×10^3 ppm SO_4^{2-}.
Solution 1: $[Cl^-] = 0$
Solution 2: $[Cl^-] = 1 \times 10^3$ ppm
Solution 3: $[Cl^-] = 1 \times 10^4$ ppm
Solution 4: $[Cl^-] = 1 \times 10^5$ ppm
†50 °C = 122 °F

polarization scan was performed. The scan started from 100 mV below the E_{corr}, scanning forward up to 800 mV above the E_{corr} and then reversing back to E_{corr}. The scanning rate was 0.167 mV/s during the forward and reverse scans. On completion of the experiments, the Cu electrodes were immediately rinsed with deionized water, dried with acetone, and examined under a microscope. Energy Dispersive X-Ray Spectroscopy (EDX) was performed only on the electrode exposed to the solution with the highest chloride concentration for element composition on surface because this solution is expected to bound any possible chloride deposition on surface.

3 EXPERIMENTAL RESULTS AND DISCUSSION

3.1 Corrosion Potential (E_{corr})

Figure 1(a) shows the E_{corr} of Cu measured prior to each EIS measurement at 50 °C [122 °F] along with previous data at 20 °C [68 °F]. The data are not continuous in some regions because of interruptions in the EIS measurement. In each solution, E_{corr} reached relatively steady values in less than 5 days. The E_{corr} values at the end of each test are plotted against Cl^- concentration in Figure 1(b), along with data points from previous work (He and Ahn, 2018). Similar to what was observed at 20 °C [68 °F], E_{corr} decreased with increasing Cl^- concentration, and in each solution, E_{corr} was 200–300 mV lower at 50 °C [122 °F] than at 20 °C [68 °F].

3.2 Potentiodynamic polarization

Figure 2(a) shows the results of cyclic polarization experiments in the 4 solutions with O_2 concentrations of about 0.1–0.2 ppb at 50 °C [122 °F]. The curves at forward and backward scans are plotted separately in Figures 2(b) and (c) for clarity. Above E_{corr}, the current increased with anodic polarization indicating anodic dissolution. For the solutions containing Cl^-, two anodic peaks on the forward scan were observed indicated by the arrows in Figure 2(b) and only one was observed in the solution without Cl^-. The numbers (1 and 2) in Figure 2(b) indicate the two stages of current change with potential separated by the first anodic peak. The different stages could be associated with the formation of different corrosion product layers on the surface as commonly observed from Cu corrosion in other environments such as O^{2-} or S^{2-} or microorganism-containing solutions (Kosec et al., 2015; Huttunen-Saarivirta et al., 2017;

Kristiansen et al., 2015; Smith et al., 2007). Beyond the peaks, there is no indication that the anodic process was suppressed by the accumulation of corrosion product deposits. On the reverse scan the current decreased with time, then switched to a cathodic reaction. The E_{corr} shown on the reverse scan was higher than on the forward scan, which could indicate surface modification by corrosion products. During both forward and

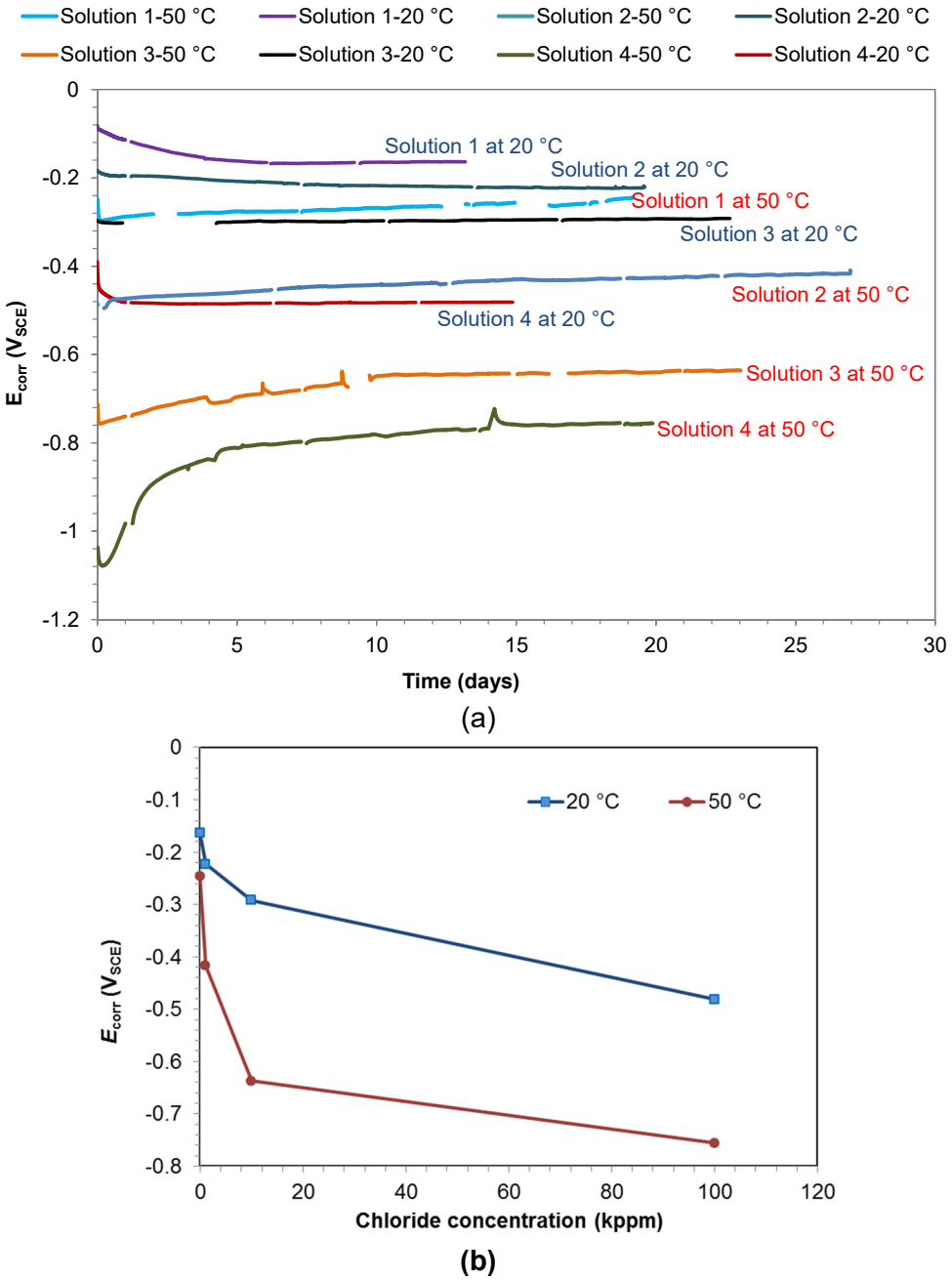

Figure 1. **(a) E_{corr} of Cu as a function of time in 4 solutions with varying Cl^- concentration and O_2 concentration of about 0.1–0.2 ppb at 50 °C [122 °F] and 20 °C [68 °F], and (b) relatively steady E_{corr} at the end of each test as a function of Cl^- concentration (Solution 1: 2×10^3 ppm SO_4^{2-}; Solution 2: 2×10^3 ppm SO_4^{2-} and 1×10^3 ppm Cl^-; Solution 3: 2×10^3 ppm SO_4^{2-} and 1×10^4 ppm Cl^-; Solution 4: 2×10^3 ppm SO_4^{2-} and 1×10^5 ppm Cl^-)**

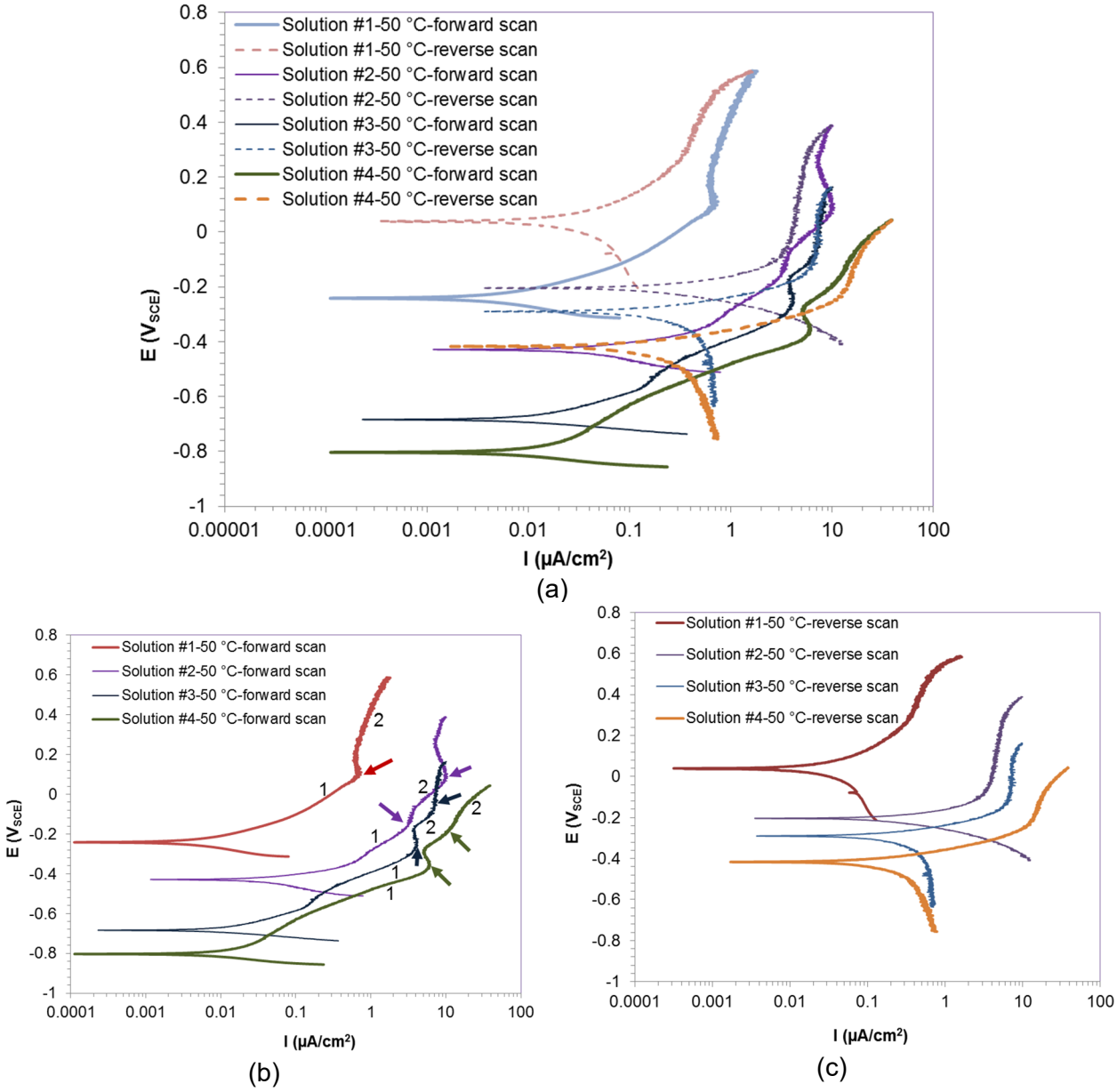

Figure 2. **Cyclic voltammograms on copper in solutions with O_2 concentration of about 0.1–0.2 ppb at 50 °C [122 °F] (a) forward and backward scans, (b) forward scan, with the arrows indicating the anodic peaks and the numbers, i.e. 1 and 2 indicating the two stages of current change with potential separated by the first anodic peak, (c) backward scan (Solution 1: 2×10^3 ppm SO_4^{2-}; Solution 2: 2×10^3 ppm SO_4^{2-} and 1×10^3 ppm Cl^-; Solution 3: 2×10^3 ppm SO_4^{2-} and 1×10^4 ppm Cl^-; Solution 4: 2×10^3 ppm SO_4^{2-} and 1×10^5 ppm Cl^-)**

reverse scans, E_{corr} consistently decreased and current density increased with increasing Cl^- concentration. Because potentiodynamic scanning was not performed on the previous tests at 20 °C [68 °F], no temperature comparison was possible.

The anodic polarization data during the forward scan show two Tafel regions, as indicated by the numbers (1 and 2) in Figure 2(b). They are fitted with the Tafel equation in Equation (1).

$$\eta = kln\frac{i}{i_0} \tag{1}$$

where η is the overpotential, k is the Tafel slope, i is the current density, and i_0 is the exchange current density. The Tafel regions and the fitting lines are shown in Figure 3. The Tafel slopes and i_0 from these four solutions are summarized in Table 2. In both regions, Tafel slopes decreased and i_0 increased significantly with increasing Cl^- concentration, indicating higher corrosion rates at higher Cl^- concentration.

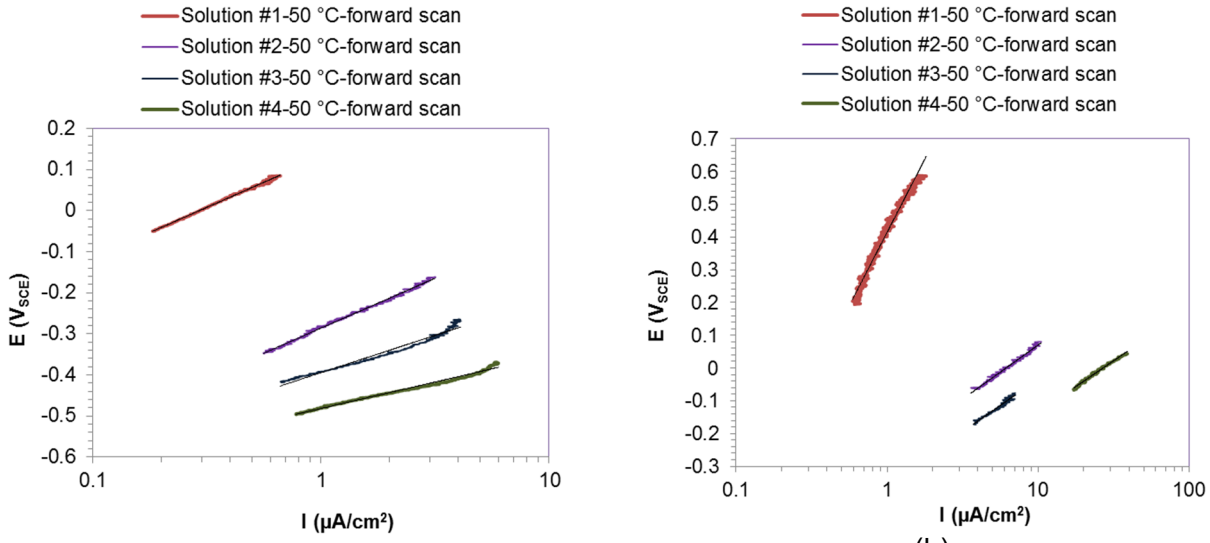

Figure 3. Tafel regions and the fit to Tafel equation for the data in forward scan (a) region 1 and (b) region 2 in Figure 2(b) (Solution 1: 2×10^3 ppm SO_4^{2-}; Solution 2: 2×10^3 ppm SO_4^{2-} and 2×10^3 ppm Cl^-; Solution 3: 2×10^3 ppm SO_4^{2-} and 2×10^4 ppm Cl^-; Solution 4: 2×10^3 ppm SO_4^{2-} and 2×10^5 ppm Cl^-)

Table 2. Tafel Slopes and Exchange Current Density for Anodic Polarization of Copper at 50 °C [122 °F]

Tafel regions	Fitting parameters	Solution 1 (2×10^3 ppm SO_4^{2-})	Solution 2 (2×10^3 ppm SO_4^{2-} and 1×10^3 ppm Cl^-)	Solution 3 (2×10^3 ppm SO_4^{2-} and 1×10^4 ppm Cl^-)	Solution 4 (2×10^3 ppm SO_4^{2-} and 1×10^5 ppm Cl^-)
Region 1	Tafel slope, mV	106	105	79	56
	i_0, μA/cm²	0.294	15.3	148	5,446
Region 2	Tafel slope, mV	388	143	140	137
	i_0, μA/cm²	0.344	6.16	12.7	26.9

3.3 EIS

Figures 4 through 7 show the EIS data obtained from four solutions with varying Cl^- concentration at different times at 50 °C [122 °F]. One set of data is compared to a set at 20 °C [68 °F]. The validity of impedance data (i.e. the dependence of magnitude and phase and the real part and imaginary part of the spectrum) was checked using the Kramers–Kronig transform. If the data is valid, equivalent circuits are used to approximate the electrochemical system. The figures include curves computed from the equivalent circuits that simulate the electrochemical system. The data showed a mix of resistive and capacitive behavior. One distinctive feature is that all the EIS spectra were different in these four solutions and they also differed from those obtained at 20 °C [68 °F].

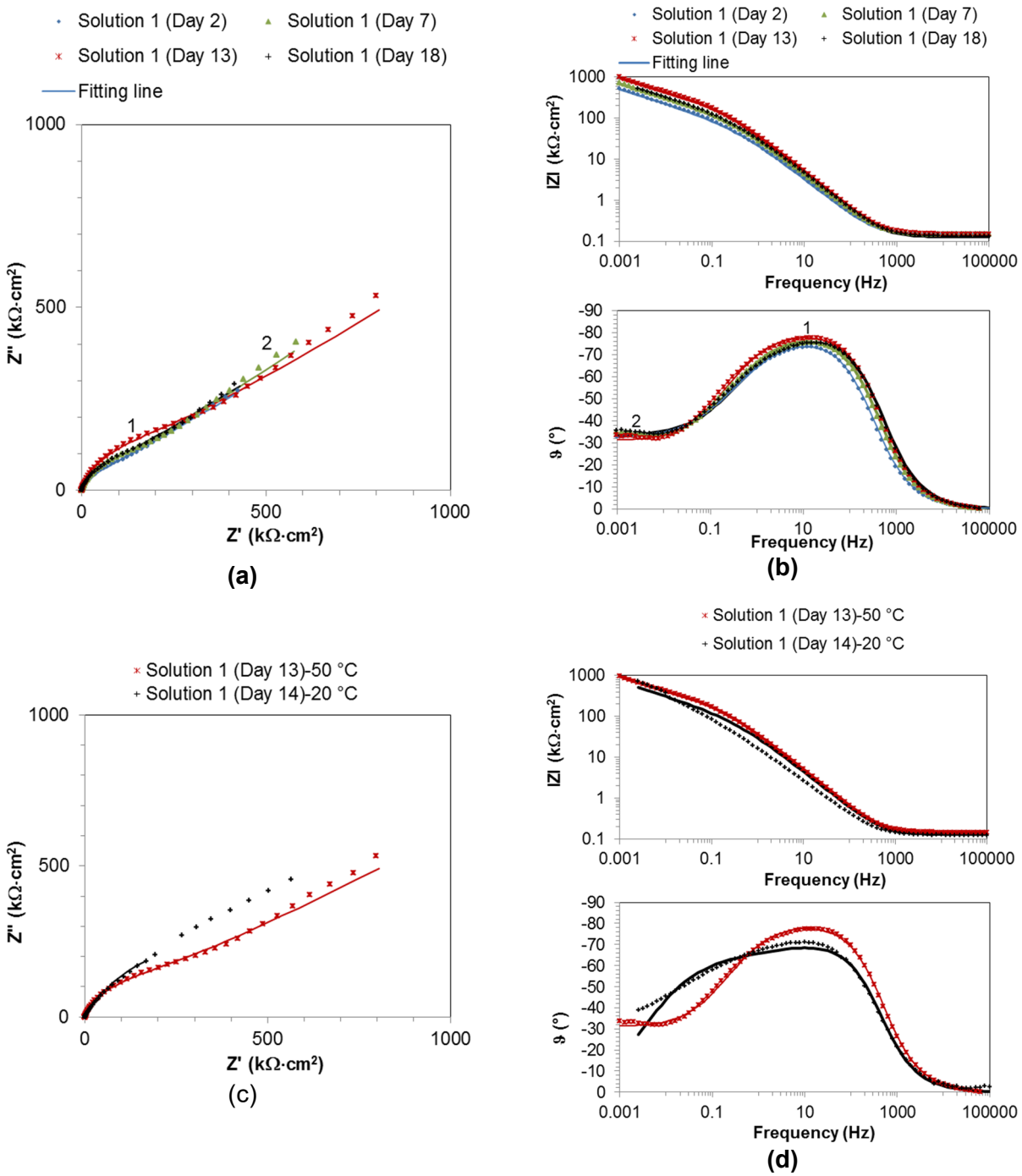

Figure 4. **EIS of Cu exposed to Solution 1 at 50 °C [122 °F] (2×10^3 ppm SO_4^{2-}) at 2, 7, 13, and 18 days; (a) Nyquist plot and (b) Bode plot. The numbers (1 and 2) in the plots are the time constants. (c) and (d) comparison with data at 20 °C [68 °F]**

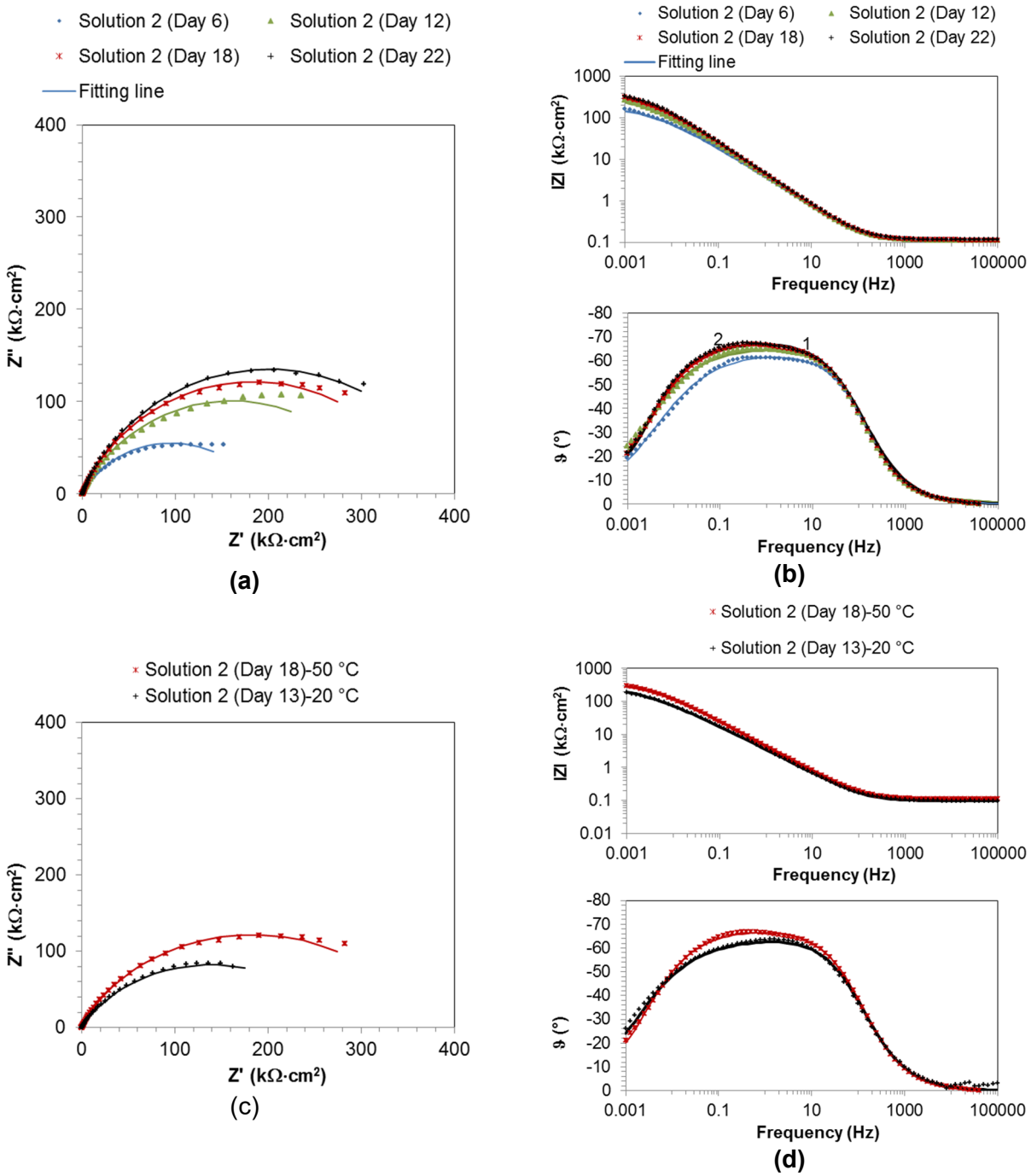

Figure 5. **EIS of Cu exposed to Solution 2 (2×10^3 ppm SO_4^{2-} and 1×10^3 ppm Cl^-) at 50 °C [122 °F] at 6, 12, 18, and 22 days; (a) Nyquist plot and (b) Bode plot. The numbers (1 and 2) in the plots are the time constants. (c) and (d) are comparison with data at 20 °C [68 °F]**

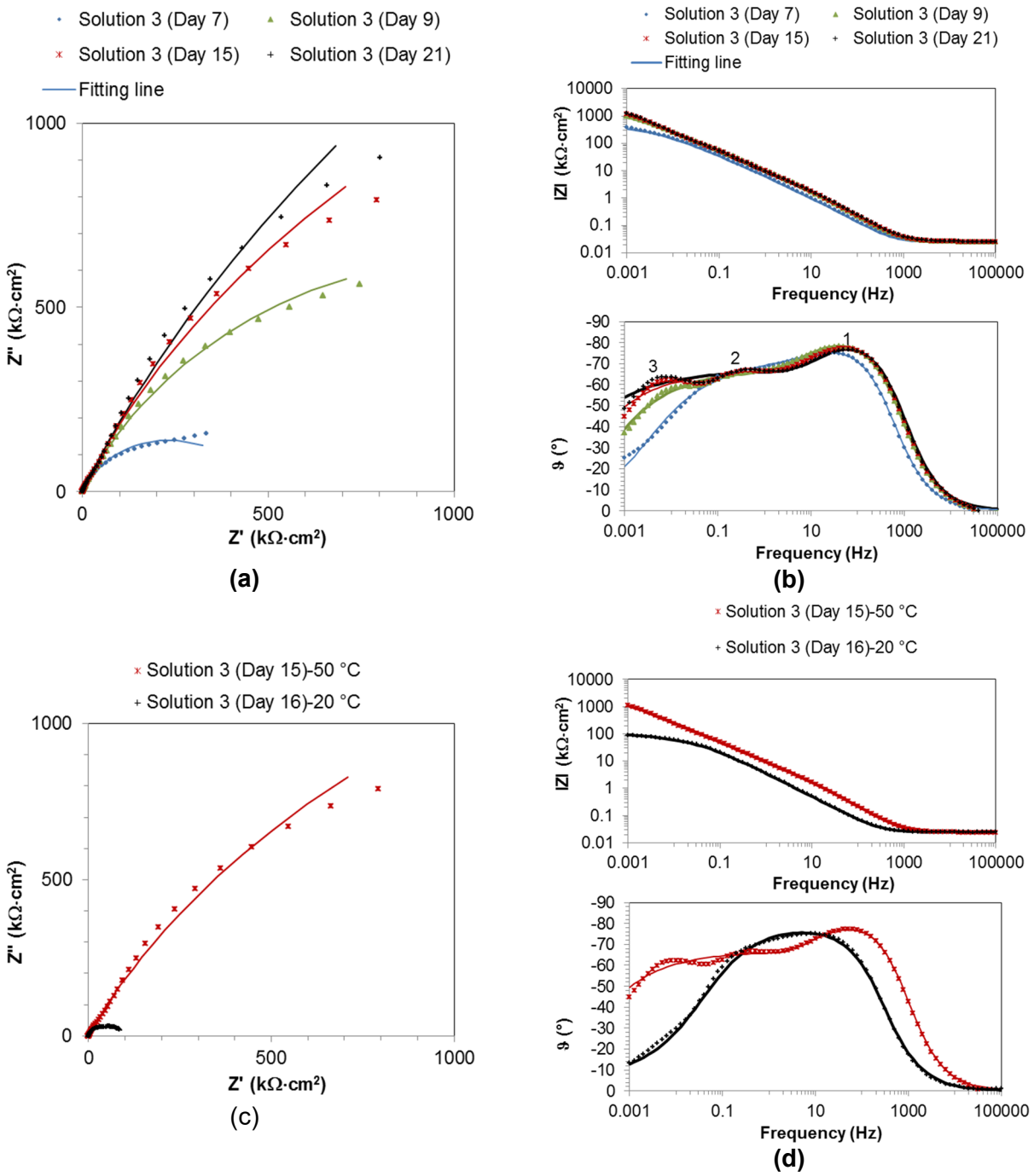

Figure 6. **EIS of Cu exposed to Solution 3 (2×10^3 ppm SO_4^{2-} and 1×10^4 ppm Cl^-) at 50 °C [122 °F] at 7, 9, 15, and 21 days; (a) Nyquist plot and (b) Bode plot. The numbers (1, 2, and 3) in the plots are the time constants. (c) and (d) are comparison with data at 20 °C [68 °F]**

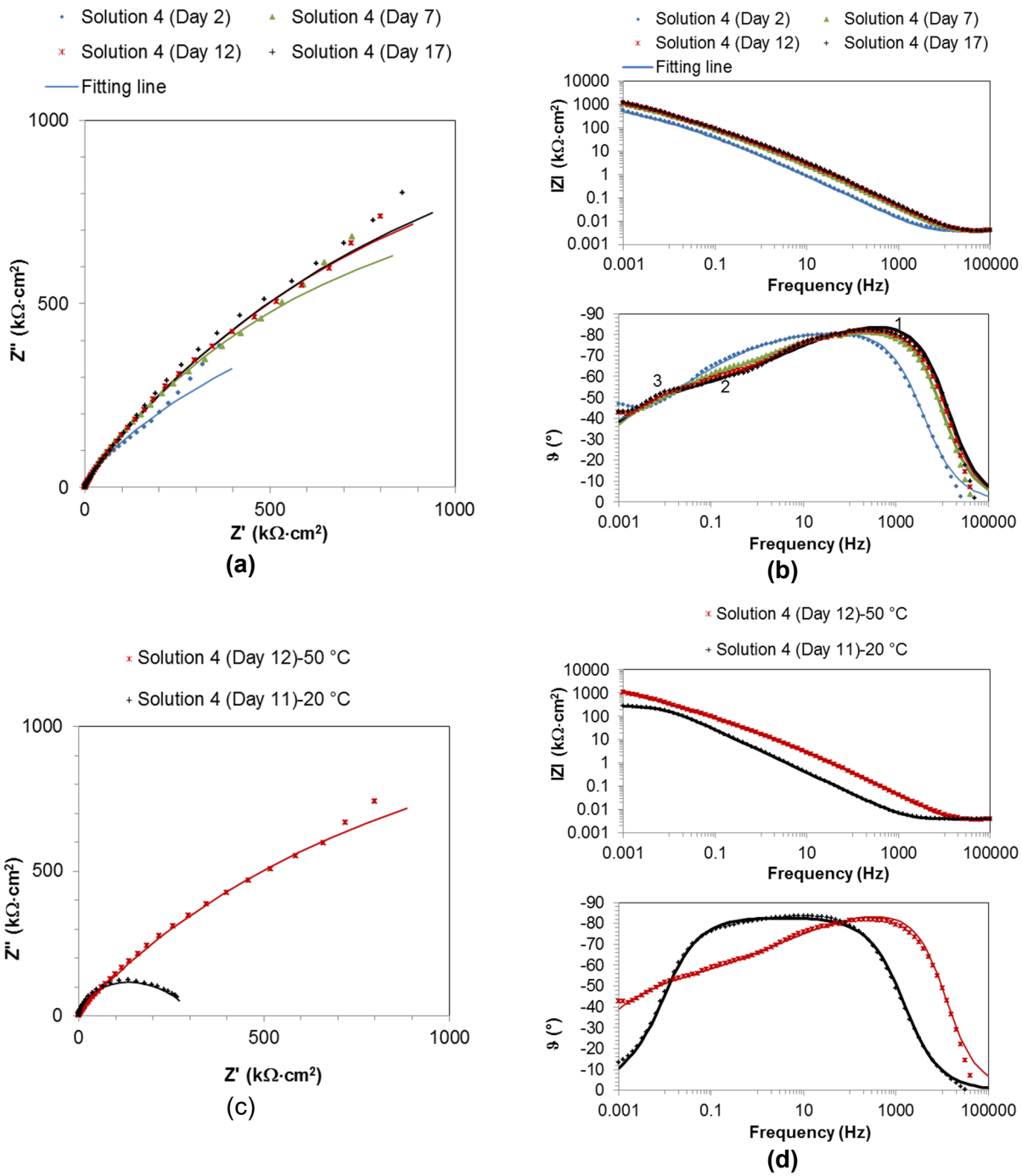

Figure 7. **EIS of Cu exposed to Solution 4 (2×10^3 ppm SO_4^{2-} and 1×10^5 ppm Cl^-) at 50 °C [122 °F] at 2, 7, 12, and 17 days at 50 °C [122 °F]; (a) Nyquist plot and (b) Bode plot. The numbers (1, 2, and 3) in the plots are the time constants. (c) and (d) are comparison with data at 20 °C [68 °F]**

The observation from each set of data is as follows:

- The EIS data from solution 1 containing SO_4^{2-} showed two time constants (τ) marked with numbers (1 and 2) in the Nyquist plot and phase angle plot in Figure 4. An equivalent electric circuit in Figure 8(a) was used to model the EIS data. This circuit consists of solution resistance (R_s), polarization resistance (R_p), film resistance (R_f), constant phase element of double layer (CPE_{dl}), and constant phase element of film (CPE_f). The physical model associated with this circuit is that there was a film on the metal surface, but the film had some discontinuities or fractures where efficient electron transfer may occur. However, the chemical composition of this film is unknown; it may be a thin layer of corrosion products. The data were well reproduced with a two-τ circuit. The fitting results are summarized in Table 3. The film resistance was extremely high, but the fitting uncertainty was also high. The computed polarization resistance corresponds to a corrosion rate in the range of tens to several nanometers per year. The corrosion rates are also included in Table 3.

- The EIS data from solution 2 containing 2×10^3 ppm SO_4^{2-} and 1×10^3 ppm Cl^- also showed two τ values, as the numbers marked in the phase angle plot in Figure 5(b). The results from fitting the two-τ circuit are in Table 3. The film resistance and polarization resistance were lower than those from solution 1, consistent with the notion that the addition of Cl^- increases corrosion rates.

- The EIS data from solution 3 containing 2×10^3 ppm SO_4^{2-} and 1×10^4 ppm Cl^- showed two τ values from the first measurement and three τ values in the remaining measurements. The τ values are marked in the phase angle plot in Figure 6(b). Changes in τ indicate changes in film structure due to extended exposure to the solution. The two-τ circuit in Figure 8(a) was used to fit the first set of data. A three-τ circuit representing two different layers of film inside the discontinuities in parallel with the double layer capacitance shown in Figure 8(b) was used to fit the data. In the physical model associated with this circuit, the film evolved with time and changed at higher Cl^- concentration. The results from fitting are in Table 3. The film resistance and polarization resistance were also lower than those from solution 1 (no Cl^- solution), indicating higher corrosion rates in solution 3.

- The EIS data from solution 4 containing 2×10^3 ppm SO_4^{2-} and 1×10^5 ppm Cl^- showed nearly three τ values, but the peaks in the phase diagram are not clearly exhibited. The τ values are marked in the phase angle plot in Figure 7(b). The data cannot be approximated well with either of the circuits in Figure 8, especially for the first set of data. It appears there was a diffusive resistance approximating 45° at low frequency. To keep the model simple, the results from fitting the two-τ circuit in Figure 8(a) are summarized in Table 3.

The averaged polarization resistance, corrosion rate, double layer capacitance, and solution resistance of Cu exposed to the four solutions at 50 °C [122 °F] derived by fitting circuits (Figure 8) to the EIS data (Figures 4 through 7) are plotted in Figure 9, along with previous data at 20 °C [68 °F]. R_p was the lowest for the solution with the highest Cl^- concentration at 50 °C [122 °F], and R_p decreased with increasing Cl^- concentration, indicating increasing corrosion rates with increasing Cl^-. The double layer capacitance was lower at 50 °C [122 °F] than at 20 °C [68 °F]. The decrease in capacitance at higher temperature could be due to layer thickening or a decrease in the dielectric constant of the double layer according to Equation (2).

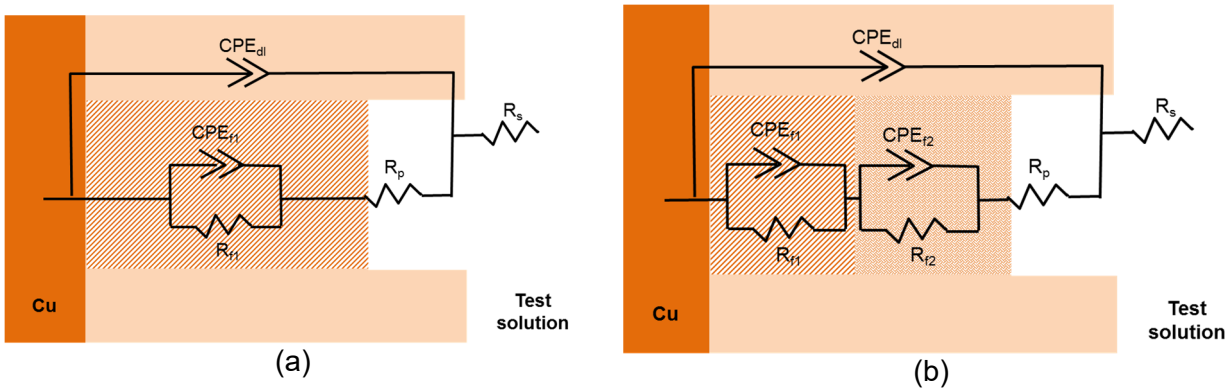

Figure 8. **(a) Two- and (b) three-time constant circuits used to model the EIS data in Figures 4 through 7 (R_s: solution resistance; R_p: polarization resistance; R_f: film resistance; CPE_{dl}: constant phase element of double layer; CPE_f: constant phase element of film)**

Table 3. Corrosion parameters and corrosion rates at 50 °C [122 °F] derived by fitting EIS to the equivalent circuits

Solution #	Time (days)	R_p (kΩ·cm^2)	R_{film1} (kΩ·cm^2)	R_{film2} (kΩ·cm^2)	C_{dl} (μF·cm^2)	R_s (Ω)	Corrosion rate calculated from R_p (nm/y)
1 (2×10^3 ppm SO_4^{2-})	2	33	4.48×10^8	N/A	7.8	16.0	19
	7	68	6.32×10^6	N/A	6.1	15.3	9.2
	13	108	8.06×10^9	N/A	4.7	15.7	5.8
	18	56	6.42×10^4	N/A	5.6	13.8	11
2 (2×10^3 ppm SO_4^{2-} and 1×10^3 ppm Cl^-)	6	1.56	196	N/A	37.0	12.3	401
	12	1.90	358	N/A	40.2	11.7	330
	18	1.91	358	N/A	40.2	11.7	328
	22	2.02	381	N/A	38.0	11.9	310
3 (2×10^3 ppm SO_4^{2-} and 1×10^4 ppm Cl^-)	7	2.98	482	N/A	20.7	2.60	210
	9	7.22	2,180	1.17	12.0	2.61	87
	15	4.08	4,517	1.17	10.9	2.62	154
	21	4.03	7,516	105	10.2	2.63	156
4 (2×10^3 ppm SO_4^{2-} and 1×10^5 ppm Cl^-)	7	0.020	768	N/A	18.5	0.334	3,697
	12	0.189	3,441	N/A	3.6	0.409	3,311
	17	0.189	5,078	N/A	3.3	0.402	3,210

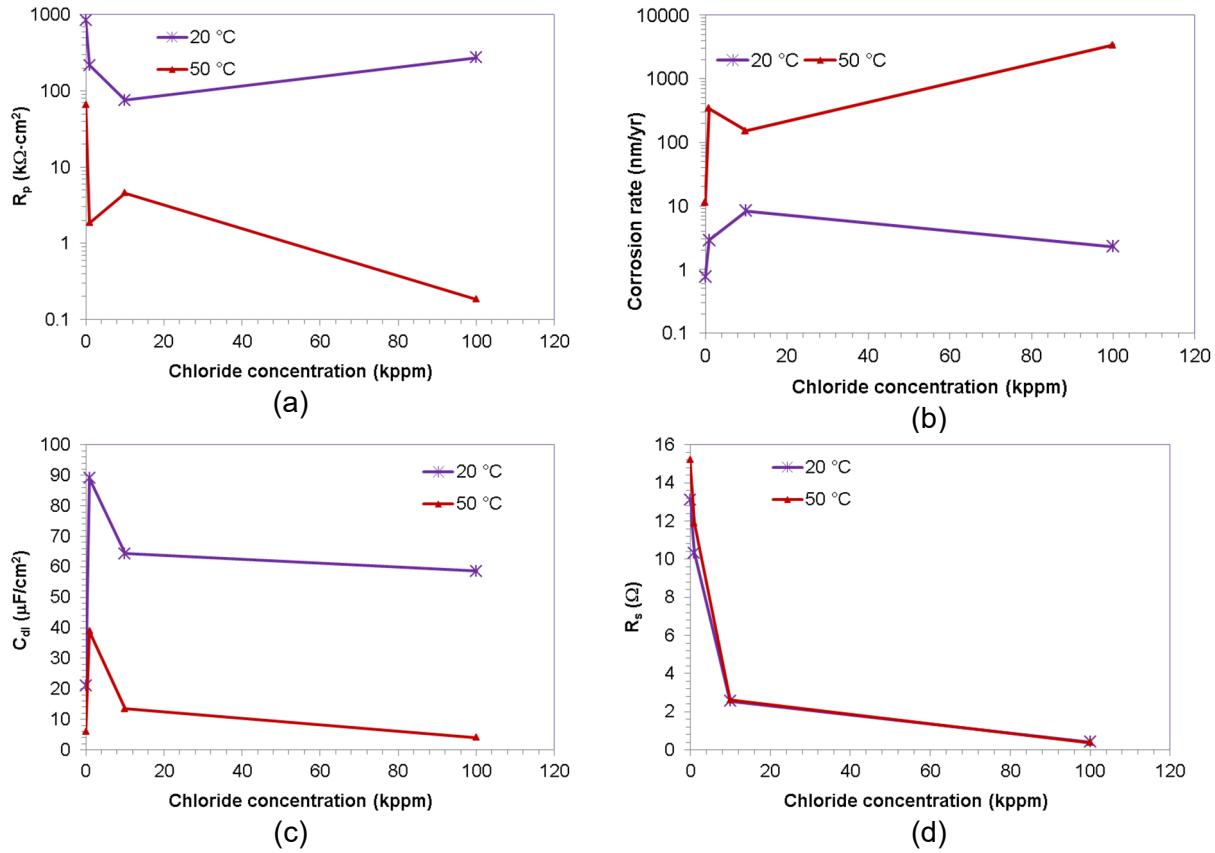

Figure 9. **Averaged (a) polarization resistance, (b) corrosion rate, (c) double layer capacitance, and (d) solution resistance of Cu exposed to four solutions at 50 °C [122 °F] derived by fitting the EIS data in Figures 4 through 7 with the model in Figure 8 and compared to previous data at 20 °C [68 °F] (He and Ahn, 2018)**

$$C = \varepsilon_0 A \frac{\varepsilon}{d} \tag{2}$$

A is the electrode surface area, ε_0 is the permitivity of free space, ε is the dielectric constant of the layer, and d is the charge separation distance. The solution resistance changed little with temperature because changes in solution resistance are dominated by solution concentration changes.

3.4 Posttest characterization

After the test, the electrodes were immediately rinsed with deionized water and dried with acetone. Optical images of posttest Cu electrodes after drying are shown in Figure 10. After the tests, all of the electrodes were slightly discolored, but no pits were observed. EDX was performed only on the electrode exposed to the solution with the highest chloride concentration. Figure 11 shows the EDX of this Cu electrode along with the untested electrode. Small amounts of silicon (Si) were present on all the specimens, very likely from the SiC grinding and polishing process for specimen preparation and from glass cell leaching. A trace amount of sulfur (S) was detected on Cu exposed to the SO_4^{2-}-containing solution, but not on the untested

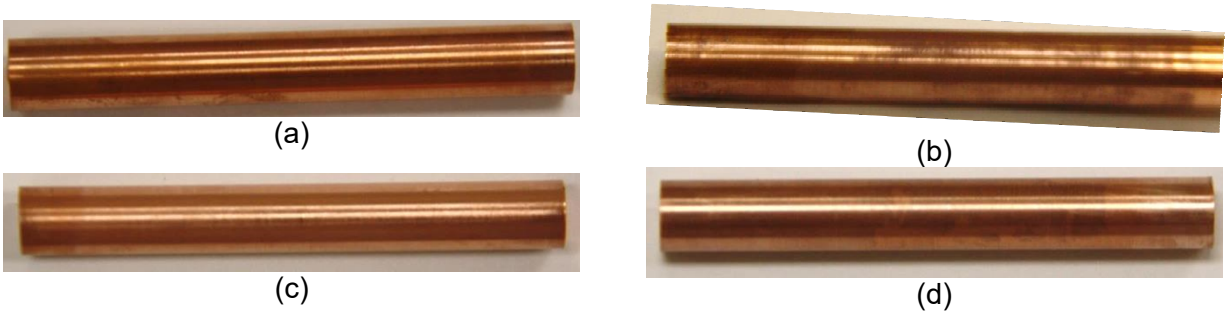

Figure 10. Optical images of Cu electrodes after exposure to (a) Solution 1 (2×10^3 ppm SO_4^{2-}), (b) Solution 2 (2×10^3 ppm SO_4^{2-} and 1×10^3 ppm Cl^-), (c) Solution 3 (2×10^3 ppm SO_4^{2-} and 1×10^4 ppm Cl^-), (d) Solution 4 (2×10^3 ppm SO_4^{2-} and 1×10^5 ppm Cl^-)

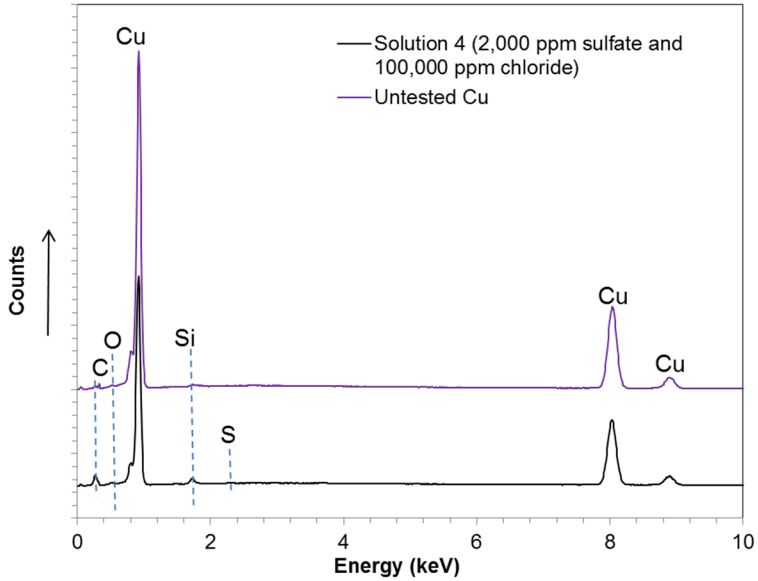

Figure 11. EDX of untested Cu and Cu electrode after exposure to solution with 2×10^3 ppm SO_4^{2-} and 1×10^5 ppm Cl^-

specimen. Chlorine (Cl) was not detected from exposure to the solution despite its high Cl^- concentration. This could be because the Cl^- is below the detection limit, or the corrosion products were rinsed off. To investigate the form of Cl^- in the corrosion products, a more sensitive ex-situ or in-situ analytical method such as Raman spectroscopy is needed.

3.5 Discussion

Literature information demonstrates that Cl^- plays a significant role in corrosion of copper, especially in oxic solutions, because Cu(I) complexation forms cuprous-chloro complex ions supported by O_2 or other cathodic reactants such as Cu^{2+} (King, 2008). The possible anodic reactions in an oxic Cl^--containing solution are:

$$Cu + Cl^- \rightarrow CuCl_{ads} + e^- \quad (3)$$

$$CuCl_{ads} + Cl^- \rightarrow CuCl_2^- \quad (4)$$

Example cathodic reactions (Betova et al., 2013) in an oxic Cl^--containing solution are:

$$O_2 + 2H_2O + 4e^- \rightarrow 4OH^- \quad (5)$$

$$Cu^{2+} + 2Cl^- + e^- \rightarrow CuCl_2^- \quad (6)$$

When exposed to oxic environments, Cu typically forms a duplex corrosion product layer, with an underlying layer of Cu_2O covered by $CuCl_2 \cdot 3Cu(OH)_2$ (King, 2008). However, in anoxic chloride containing solutions, some studies show no evidence for Cu corrosion (Simpson and Schenk, 1987; Eriksen et al., 1989; Hedin et al., 2014). Research sponsored by SKB (Hedin, et al., 2014) showed that the following cathodic reaction producing H_2 is not a thermodynamically feasible path to support Cu corrosion in anaerobic neutral solutions because the H^+/H_2 equilibrium potential is lower than the Cu^+/Cu and Cu^{2+}/Cu equilibrium potential in the Pourbaix diagram (Pourbaix, 1974), except at some extreme conditions that the equilibrium potentials change order:

$$2H_2O + 2e^- \rightarrow H_2 + 4OH^- \quad (7)$$

Figures 1 and 2 and Tables 2 and 3 show that E_{corr} decreased, anodic current density increased, Tafel slope decreased, exchange current density increased, and corrosion rate increased with increasing Cl^- concentration. E_{corr} also decreased with increasing temperature. All these results consistently demonstrate that Cl^- played a significant role in enhancing corrosion of copper in solutions with O_2 concentrations of 0.1–0.2 ppb. Figure 12 illustrates schematically the Tafel approximation for the polarization curves for both the cathodic and anodic reactions. Higher temperature and higher Cl^- concentration could have depolarized the anodic reaction, resulting in lower E_{corr} values and potentially larger i_{corr}.

The EIS data in Figures 4 through 7 suggest a layered film structure on the metal surface. This could indicate the formation of Cu_2O or $CuCl_2 \cdot 3Cu(OH)_2$ as those are observed in oxic solutions. However, all of these observations seem to be in conflict with information in the literature reporting lack of Cu corrosion in anaerobic solutions. It is uncertain what the cathodic reaction is in this work. There are several possibilities for cathodic reactions: (i) reduction of trace amounts of O_2 in solution, (ii) reduction of Cu^{2+} in the air-formed oxide, (iii) reduction of H_2O to H_2 catalyzed by Cu^{2+}, and (iv) reduction of SO_4^{2-} to S^{2-} assisted by sulfate reducing bacteria as S was observed in the EDX analyses (Figure 11). At high Cl^- concentration, the kinetic rate is

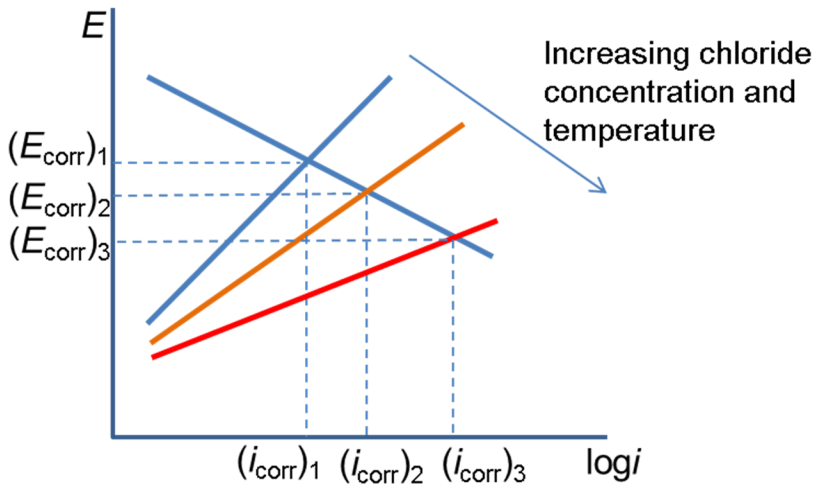

Figure 12. Effect of increasing Cl^- concentration on the E_{corr} and corrosion tendency (The blue, orange, and red colors of the lines illustrate the increasing Cl^- concentration and temperature)

high (indicated by the large exchange current density) and the controlling factor could be diffusion of cathodic reactants. Comparison of data in Figures 4–7 shows that the magnitude of the impedance at 50 °C [122 °F] was higher than at 20 °C [68 °F]. This could be because the film formed at higher temperature is resistive over the testing period. However, it is uncertain whether the film would maintain its resistivity over a long time period. Further work is needed to evaluate the cathodic reactions, the film, and the corrosion products using more sensitive analytical methods over longer times and to reconcile the results with information in the literature.

4 SUMMARY

This study investigated the role of Cl^- in Cu corrosion in solutions containing SO_4^{2-} and Cl^- with residual O_2 concentrations of about 0.1–0.2 ppb at 50 °C [122 °F]. SO_4^{2-} concentration was kept constant at 2×10^3 ppm, while Cl^- concentration was varied from 0 to 1×10^3, 1×10^4, and 1×10^5 ppm. Electrochemical methods, including E_{corr} monitoring, potentiodynamic polarization, and EIS, were used to study the Cu corrosion properties.

After immersing the electrode in solution, E_{corr} reached relatively steady values in several days. E_{corr} decreased with increasing Cl^- concentration and increasing temperature. Under potentiodynamic polarization, the current increased with anodic polarization, and anodic peaks on the forward scan were observed in the solutions containing Cl^-. Beyond the peaks, there is no indication that the anodic process is suppressed by the accumulation of corrosion product deposits. During both forward and reverse scans, E_{corr} consistently decreased and the current density increased with increasing Cl^- concentration. Tafel slopes decreased and exchange current density also increased with increasing Cl^- concentration. The EIS data differed in solutions with different Cl^- concentrations and also differed from those obtained at 20 °C [68 °F]. Two and three time constants, indicating a layered film structure, were determined from the EIS data. The polarization resistance derived by fitting equivalent circuits to the EIS data decreased with increasing Cl^- concentration.

All these results obtained using different methods consistently demonstrate that Cl^- plays a significant role in enhancing corrosion of copper in these solutions with extremely low O_2 concentrations. Higher temperature and higher Cl^- concentration could have depolarized the anodic reaction, resulting in lower E_{corr} values and potentially larger i_{corr}. However, the corrosion products have not been identified and it is therefore uncertain what they imply regarding long-term Cu performance in repository conditions. The nature of the cathodic reaction supporting the corrosion process is also uncertain. Further work is needed to evaluate the cathodic reactions and corrosion products using more sensitive analytical methods to reconcile the results with information in the literature.

5 REFERENCES

Betova, I., M. Bojinov, and C. Lilja. "Long-Term Interaction of Copper with a Deoxygenated Neutral Aqueous Solution." *Journal of the Electrochemical Society.* Vol. 160. pp. C49–C58. 2013.

Eriksen, T.E., P. Ndalamba, and I. Grenthe. "On the Corrosion of Copper in Pure Water." *Corrosion Science*. Vol. 29. pp. 1,241–1,250. 1989.

He, X. and T. Ahn. "Effects of Chloride on Copper Corrosion and Cathodic Charging of Carbon Steel for Nuclear Waste Disposal Application." Washington, DC: U.S. Nuclear Regulatory Commission. 2018.

He, X. and T. Ahn. "Experiments on Corrosion of Copper and Carbon Steel Waste Containers—Progress Report for Fiscal Years 2015 and 2016." ML17003A453. Washington, DC: U.S. Nuclear Regulatory Commission. 2017.

He, X., T. Ahn, and J. McMurry. "Literature Review and Experiments on Waste Package Corrosion—Copper and Carbon Steel." ML16014A269. Washington, DC: U.S. Nuclear Regulatory Commission. 2015.

Hedin, A., C. Lilja, and J. Johansson. "Copper Corrosion in Oxygen Free Water—Status Report." SKB Document ID 1457600. 2014.

Huttunen-Saarivirta, E., P. Rajala, M. Bomberg, and L. Carpén. "EIS Study on Aerobic Corrosion of Copper in Groundwater: Influence of Microorganisms." *Electrochimica Acta*. Vol. 240. pp. 163–174. 2017.

King, F. "Theory Manual for the Copper Corrosion Model for Uniform Corrosion in Sedimentary Rock CCM-UC.1.1." NWMO TR-2008-07. Toronto, Ontario, Canada: Nuclear Waste Management Organization. 2008.

King, F. "Container Materials for the Storage and Disposal of Nuclear Waste." *Corrosion*. Vol. 69. pp. 986–1,011. 2013.

Kosec T., Z. Qin, J. Chen, A. Legat, and D.W. Shoesmith. "Copper Corrosion in Bentonite/Saline Groundwater Solution: Effects of Solution and Bentonite Chemistry." *Corrosion Science*. Vol. 90. pp. 248–258. 2015.

Kristiansen, P.T., F. Massel, L. Werme, C. Lilja, and L.C. Duda “Sulfidation of Single-Phase Oxide on Copper and as Powder Studied Using Soft X-Ray Spectroscopy.” *Journal of the Electrochemical Society*. Vol. 162. pp. C785–C791. 2015.

Pourbaix, M. Atlas of Electrochemical Equilibria in Aqueous Solutions. 2nd edition. Houston, TX: NACE International. 1974.

Sander, R. “Compilation of Henry’s Law Constants (version 4.0) for Water as Solvent.” *Atmospheric Chemistry and Physics*. Vol. 15. pp. 4399–4981. 2015.

Simpson, J.P. and R. Schenk. “Hydrogen Evolution from Corrosion of Pure Copper.” *Corrosion Science*. Vol. 27. pp. 1,365–1,370. 1987.

Smith, J., Z. Qin, F. King, L. Werme, and D.W. Shoesmith. “Sulfide Film Formation on Copper Under Electrochemical and Natural Corrosion Conditions.” *Corrosion*. Vol. 63. pp. 135–144. 2007.